Linking polar amplification and midlatitudes eddy heat flux trends

Rei Chemke[1] & Lorenzo M. Polvani[1,2]

[1]*Department of Applied Physics and Applied Mathematics, Columbia University, New York, NY 10027, USA*

[2]*Department of Earth and Environmental Sciences, and Lamont-Doherty Earth Observatory, Columbia University, Palisades, NY 10964, USA*

Eddy heat fluxes play the important role of transferring heat from low to high latitudes, thus affecting midlatitude climate. The recent and projected polar warming, and its effects on the meridional temperature gradients, suggests a possible weakening of eddy heat fluxes. We here examine this question in reanalyses and state-of-the-art global climate models. In the Northern Hemisphere we find that the eddy heat flux has robustly weakened over the last four decades. We further show that this weakening emerged from the internal variability around the year 2000, and attribute it to greenhouse gas emissions. In contrast, in the Southern Hemisphere we find that the eddy heat flux has robustly strengthened, and we link this strengthening to the recent multi-decadal cooling of Southern-Ocean surface temperatures. The inability of state-of-the-art climate models to simulate such cooling prevents them from capturing the observed Southern Hemisphere strengthening of the eddy heat flux. This discrepancy between models and reanalyses provides a clear example of how model biases in polar regions can affect the midlatitude climate.

Main

One of the largest signals of climate change in recent and future decades is polar amplification: the stronger low-level warming of the poles relative to lower latitudes[1,2]. Such an amplification acts to reduce the meridional temperature gradient, and several studies have suggested that the recent Arctic amplification has affected midlatitudes extreme weather[3–6]. However, while no one disputes the existence Arctic amplification in recent decades, there is still much debate regarding its effects on midlatitudes, since such effects are difficult to separate from the large internal climate variability[7–16]. Here we investigate a new aspect of the possible connection between high latitude temperature changes and the midlatitude circulation: the eddy heat flux, which, as shown below, exhibits robust and clear trends over the last several decades.

Eddy heat fluxes have large climatic impacts at midlatitudes. Not only do they play an integral role in transferring heat from low to high latitudes, but also in driving the mean meridional circulation, and in the initial stages of baroclinic eddy life cycles[17–19]. To better understand the behavior of midlatitude eddies, many previous studies have tried to relate eddy fluxes to the gradient of the mean fields. For example, using arguments from linear baroclinic instability theory, several studies[20–22] have tried to relate changes in Eady growth rate to changes in the eddy fields (eddies are argued to have a direct relation to the mean temperature gradient). The relation between the eddies and the mean gradient was also studied using simple diffusive closures[19,23–25], where the poleward eddy fluxes are assumed to be proportional to the mean meridional gradient, for example, $\overline{v'T'} \propto -\overline{T}_y$, where v is meridional velocity, T is temperature, the subscript y denotes meridional derivative, and over-bar and prime denote mean and eddy terms, respectively. Such closures are

also commonly used in baroclinic adjustment theories, where the eddy fluxes act to stabilize the baroclinically unstable flow, and keep it marginally supercritical to baroclinic instability[26,27].

Eddy heat fluxes are known to be more sensitive to lower level changes in temperature gradient rather than to upper level changes[28,29], as long as the baroclinicity (temperature gradients) is concentrated in the lower levels of the atmosphere, and is not controlled by changes in static stability[30]. Thus, the recent (and projected) anthropogenic-induced Arctic amplification would imply a decline in Northern Hemisphere (NH) meridional eddy heat flux, as a smaller heat transport is required to maintain a weaker temperature gradient. In the Southern Hemisphere (SH), on the other hand, the recent multi-decadal Southern Ocean cooling would imply a strengthening of eddy heat flux. The aim of this work is thus to examine the recent trends in midlatitude eddy heat flux, their connection to recent changes in high latitude temperatures, and the role of anthropogenic emissions in those trends.

Southern Hemisphere

It is instructive to start by considering the hemisphere where polar amplification has, to date, not been observed. Fig. 1a shows the SH 1979-2017 annual eddy heat fluxes ($\overline{v'T'}$, calculated from daily data, Methods) trends in 13 models of the Coupled Model Intercomparison Project Phase 5 (CMIP5) and in three different reanalyses (Methods). We here use the absolute value of $\overline{v'T'}$, so that positive (negative) values indicate strengthening (weakening) in both hemispheres. CMIP5 models (blue bars) show large spread in $\overline{v'T'}$ trends: half of the models simulate a strengthening over the last four decades, while the other half simulate a weakening. As a result, the multi-model mean (purple bar) show no trend at all. In contrast, the reanalyses (green bars) show a

robust strengthening of $\overline{v'T'}$, which is only captured by a few models. This discrepancy between reanalyses and models can be further seen in the time evolution, relative to the 1979-1989 period, of $\overline{v'T'}$ (Fig. 1c): the strengthening in reanalyses is not captured by climate models, which in fact show a monotonic weakening until the end of the 21st century. We next address this discrepancy, and elucidate why climate models show such a large spread while reanalyses do not.

Model spread could stem from two sources: internal variability of the climate system or differences in the model formulations. To determine whether internal variability explains the spread across the models, we make use of the Community Earth System Model (CESM) large ensemble (LE) (Methods). Fig. 1b is similar to Fig. 1a but shows the 1979-2017 trends in $\overline{v'T'}$ for 40 individual LE members (red bars), and the same reanalyses (green). Most LE members (36) simulate a weakening of $\overline{v'T'}$. Only four members show a strengthening, and it is considerably weaker than the strengthening in the reanalyses. This suggests that internal variability is likely not the main reason for the large spread across the CMIP5 models, and their discrepancy with the reanalyses. Note that since the mean of the LE (yellow bar) represents the model's forced response to anthropogenic emission (as the internal variability is averaged out), the simulated weakening of $\overline{v'T'}$ is part of the forced response, which is projected to continue in coming decades, as can be clearly seen in the time evolution of the LE (Fig. 1d).

We next examine the role of the different model formulations in the modeled trends of $\overline{v'T'}$. As discussed in the introduction, one expects a strong coupling between $\overline{v'T'}$ and the meridional near-surface air temperature (SAT) gradient: it is thus tempting to relate the discrepancy in $\overline{v'T'}$ trends between reanalyses and models to the models' inability to capture the recent multi-decadal

cooling of the Southern-Ocean surface temperature[31–33]. To determine if this relation exists, we start by showing in Fig. 2a the correlation between trends in $\overline{v'T'}$ and trends in the meridional gradient of SAT ($\Delta_y \mathrm{SAT}$, estimated as the difference between low, $20°\mathrm{S} - 40°\mathrm{S}$, and high latitudes, $55°\mathrm{S} - 75°\mathrm{S}$) in CMIP5 models (blue), LE members (red) and reanalyses (green). The 39-year trends in $\overline{v'T'}$ is highly correlated with trends in $\Delta_y \mathrm{SAT}$, with $r = 0.92$ across the CMIP5 models (and $r = 0.87$ when including the LE members and reanalyses as well). Not only a good correlation exists between these two quantities, but CMIP5 models which show positive trends in $\overline{v'T'}$ (open blue dots) also show positive trends in $\Delta_y \mathrm{SAT}$, whereas CMIP5 models which show negative trends in $\overline{v'T'}$ (filled blue dots) also show negative trends in $\Delta_y \mathrm{SAT}$. Similarly, most LE members show negative trends in both $\overline{v'T'}$ and in $\Delta_y \mathrm{SAT}$. The reanalyses, which show positive trends in $\overline{v'T'}$, also show positive trends in $\Delta_y \mathrm{SAT}$.

Next we ask: does the spread in trends in $\Delta_y \mathrm{SAT}$ stem from high or low latitudes SAT trends? To answer this, we decompose the trends in $\Delta_y \mathrm{SAT}$ into trends in low and high latitudes SAT separately (Fig. 2c). This shows that most of the spread in $\Delta_y \mathrm{SAT}$ indeed stems from high latitude temperature trends: while all models and reanalyses show a comparable and positive low-latitude warming trend of $\sim 0.01\,\mathrm{Kyr}^{-1}$ (y-axis in Fig. 2c), models with high-latitude warming stronger than their low latitude warming (situated below the 1:1 dot-dashed line) show negative trends in $\Delta_y \mathrm{SAT}$ and in $\overline{v'T'}$ (filled blue and red dots), whereas models with high latitude warming weaker than their low latitude warming (situated above the 1:1 dot-dashed line) show positive trends in $\Delta_y \mathrm{SAT}$ and in $\overline{v'T'}$ (open blue dots). Unlike most models, reanalyses show high latitude cooling trends over the last decades (green dots), which are consistent with the robust positive

trends in $\Delta_y \mathrm{SAT}$ and in $\overline{v'T'}$ (Fig. 2a). Although causality arguments cannot be made based on correlation alone, these results clearly suggest that the model spread in $\overline{v'T'}$ trends, and their partial inability to capture the $\overline{v'T'}$ trends in reanalyses, might indeed stem from biases in simulated surface temperature at high latitudes.

To further examine the model biases in high latitude temperature, and to ascertain whether the reanalyses are indeed unaffected by such biases (reanalyses might also have biases in model formulations), we next compute temperature trends from observational data sets that are untainted by any model biases: we show the NOAAGlobalTemp, GISTEMP and HadCRUT4 trends (gray dashed lines and gray dots in Fig. 2a and c, respectively) (Methods). The high latitude cooling and the positive trends in $\Delta_y \mathrm{SAT}$ in reanalyses are also present in all three observational data sets. Given the good correlation between $\Delta_y \mathrm{SAT}$ and $\overline{v'T'}$, this agreement between the reanalyses and observations further corroborates our interpretation that the robust observed strengthening of $\overline{v'T'}$ is not an artifact of the reanalyses, and that the large spread across the models stems from biases in temperature at high southern latitudes. Interestingly, the fact that some models do not capture the high latitude cooling but do show positive trends in $\overline{v'T'}$ (open blue dots) indicates that in order for high latitude model biases in surface temperature to affect $\overline{v'T'}$ at midlatitudes it needs to be large enough to change the sign of the temperature gradient trend.

Finally, we demonstrate that if one corrects the models' surface temperature biases one obtains the same robust strengthening of $\overline{v'T'}$ found in the reanalyses. For this we make use of a 10-member ensemble of CESM atmosphere-only runs (Global Ocean Global Atmosphere, LE-GOGA) simulations, which prescribed observed surface temperature (Methods). Fig. 2b is similar

to Fig. 1b but shows the last available 37-year (1979-2015) trends in $\overline{v'T'}$ in both the LE-GOGA and reanalyses. Unlike the ocean-atmosphere coupled LE runs, which show a weakening in $\overline{v'T'}$, when the sea surface temperatures (SSTs) and sea-ice are prescribed from observations all members show a strengthening in $\overline{v'T'}$ (red bars), similar to the strengthening in the reanalyses (green bars). The strengthening of $\overline{v'T'}$ across all GOGA members can be further seen in the time evolution of $\overline{v'T'}$, which accompanies the evolution in the reanalyses (Fig. 2d). This confirms our interpretation that high latitude biases in simulated surface temperature affect the midlatitude climate trends.

Northern Hemisphere

In contrast to the robust observed strengthening in the SH, $\overline{v'T'}$ in the NH reanalyses show a robust weakening over the last four decades (1979-2017) (green bars in Fig. 3a). Relative to the 1979-1989 period, by 2017 $\overline{v'T'}$ has weakened by $\sim 6\%$, and is projected to weaken by $\sim 20\%$ by the end of the 21st century (Fig. 3c). In addition, unlike the large model spread in the SH, in the NH most CMIP5 models agree on the sign of trends, and also simulate a robust weakening between 1979-2017 (blue bars in Fig. 3a). As a result the multi-model mean (purple bar) also shows a weakening of $0.01\,\mathrm{Kms}^{-1}\mathrm{yr}^{-1}$. As discussed in the introduction, such a weakening is consistent with the reduction in the meridional temperature gradient and warming of the Arctic. Fig. 4a shows that the weakening of $\overline{v'T'}$ is also correlated with the reduction in $\Delta_y\mathrm{SAT}$ (estimated as the difference between low, $20°\mathrm{N}-40°\mathrm{N}$, and high latitudes, $65°\mathrm{N}-85°\mathrm{N}$) with $r = 0.62$ across the CMIP5 models (and $r = 0.51$ when including the LE members and reanalyses as well). As in the SH, the spread in $\Delta_y\mathrm{SAT}$ is mostly due to the warming of high latitudes (Arctic), and not due

147 to the warming of low latitudes (Fig. 4c). The lower correlation between $\overline{v'T'}$ and $\Delta_y \mathrm{SAT}$ in the
148 NH than in the SH may be related to the fact that the longitudinal distribution of Arctic warming
149 is different than that of $\overline{v'T'}$, and from the effects of static stability on $\overline{v'T'}$[30].

150 Is the NH weakening of $\overline{v'T'}$ is part of the forced response to anthropogenic emissions, or
151 merely part of the internal variability of the climate system? First, the fact that all CMIP5 models
152 project that such a weakening will continue in coming decades (Fig. 3c) suggests that the recent
153 decline in reanalyses constitutes part of the emerged forced response to anthropogenic emissions.
154 Second, in order to quantitatively answer such a question one has to disentangle the forced response
155 from the internal variability. Thus, we again make use of the CESM LE, where the spread across its
156 members is due to internal variability alone, and the mean of the ensemble is the forced response.

157 Fig. 3b shows the NH $\overline{v'T'}$ 1979-2017 trends in the LE members (red) and reanalyses (green).
158 Similar to the reanalyses and CMIP5 models, all LE members (except one) show a weakening in
159 $\overline{v'T'}$. As a result, the mean of the LE (yellow bar) also shows a weakening, which is approximately
160 half of the weakening in the reanalyses. Assuming that the LE realistically simulates the internal
161 variability of the climate system, this would indicate that the recent decline in $\overline{v'T'}$ is partially (half)
162 due to anthropogenic emissions: the other half is due to internal variability. As the weakening is
163 projected to continue in coming decades across all LE members (Fig. 3d), one suspects that the
164 recent decline might constitutes the emergence of the forced response to anthropogenic emissions.
165 We next analyze this question.

166 The "time of emergence" has been used in previous studies to identify when a forced signal
167 appears as distinct from the internal variability (the noise)[34,35]. While different studies have used

different definitions for the signal and the noise, in all studies the time of emergence is estimated as the time when the signal exceeds a certain threshold (usually one standard deviation) of the internal variability, defined as the noise. To assess whether an anthropogenic signal can be detected in the recent trends of $\overline{v'T'}$ we here use two different approaches for estimating the time of emergence.

In the first, following previous studies[35], we use the time evolution relative to a reference period (here we choose 1979-1989) of the LE in order to define the signal and the noise. The signal is defined as the time evolution of the LE mean, and the noise as the time evolution of one standard deviation across all members. Using this approach the forced signal emerges out of the internal variability by 2009.

In the second approach we estimate the time of emergence for each realization separately, in both the LE and reanalyses, by comparing the signal to a distribution that lacks the forced response[34,36]. The signal is computed as trends over different lengths in each realization, and the noise as one standard deviation across all trends with corresponding lengths in the CESM preindustrial control run (Methods). Following previous studies[36], we use this same noise for calculating the time of emergence in both the LE and reanalyses. The trends are first calculated for each member and reanalysis over 10 years (from 1979 to 1988) and then over consecutive lengths of trends (from 1979 to 1989,1990...) until the signal emerges.

Fig. 4b shows the distribution of the time of emergence across the LE members (red bars). By 2010 most (74%) of the LE members show that the signal has emerged. The mean of the LE emerges by 2009 (yellow vertical line), which is similar to the emergence of the forced response estimated by the first approach. Not only the LE shows that the signal of the weakening in $\overline{v'T'}$

has already emerged, but also the reanalyses: the green vertical lines in Fig. 4b show that in all reanalyses the weakening in $\overline{v'T'}$ has already emerged out of the internal variability during the 90's. By 2017 $\overline{v'T'}$ trends in reanalyses could not be explained using the sole presence of internal variability, attesting they constitute the forced signal (Supplementary Fig. 2). Calculating both the signal and noise of the reanalyses using their time evolution[34], rather than using the preindustrial control run, yields the same time of emergence.

Is the forced signal that has been detected in the recent weakening of NH $\overline{v'T'}$ anthropogenic or natural? To answer that we make use of a 20-member ensemble, which is identical to the LE simulations, but forced without the time varying greenhouse gases (LE-fixGHG, Methods). We start by showing the LE-fixGHG mean time evolution, relative to the 1979-1989 period, of $\overline{v'T'}$ (black line in Fig. 3d). Fixing the greenhouse gases results in no forced $\overline{v'T'}$ weakening in NH in recent and coming decades, attesting that the recent observed weakening in $\overline{v'T'}$ can be attributed to the increase in greenhouse gases. Similarly, comparing the observed 1979-2017 trends in NH $\overline{v'T'}$ with the trends in the LE and LE-fixGHG shows that without the time varying greenhouse gases one cannot explain the recent weakening in NH $\overline{v'T'}$ (Fig. 4d).

In summary, if the recent changes in $\overline{v'T'}$ (weakening in NH and strengthening in SH) are to continue in coming decades, they will further impact the midlatitudes climate as $\overline{v'T'}$ are a major player in midlatitudes circulation. Moreover, since $\overline{v'T'}$ trends are linked to polar temperature trends, it will be important to correct the high latitude temperature trend biases in the models, specifically in the SH, in order to produce accurate projections of midlatitudes climate.

Methods

To examine the recent behavior of the annual eddy heat fluxes in reanalyses and models we make use of daily temperature and meridional wind data, and compute $\overline{v'T'}$, where bar and prime denote zonal and monthly averages, and deviation therefrom, respectively. As $\overline{v'T'}$ is maximum at midlatitudes and in the lower part of the troposphere we average it from the surface to 700 mb and between $40^\circ - 70^\circ$ in the NH, and between $40^\circ - 60^\circ$ in the SH. We limit the averaging in the SH to 60° in order to avoid artificial near-surface values in pressure interpolated fields over the Antarctic continent (Supplementary Fig. 1).

Reanalyses

The eddy heat flux is analyzed across 4 different reanalyses: The ECMWF Era-Interim[37] (ERA-I), NCEP/DOE Reanalysis II[38], JRA-55[39], and CFSR V2[40]. Due to strong biases in SH midlatitude eddies[41–43], we here only analyze the NCEP data in the NH.

CMIP5 models

We also analyze 13 models that participate in the Coupled Model Intercomparison Project Phase 5[44] (CMIP5), between 1950-2100 under the historical and RCP8.5 scenarios (Supplementary Table 1). Although a few models other than those listed have made daily data needed for calculating $\overline{v'T'}$ available, those models show large low-level biases in $\overline{v'T'}$, and thus we have excluded them from our analysis.

Large ensemble of model simulations

In order to disentangle the forced response to anthropogenic emissions from internal variability, and determine whether recent trends have emerged out of the internal variability, we analyze four

experiments with the Community Earth System Model (CESM). The first, is an ocean-atmosphere coupled large ensemble (LE) that consists 40 simulations (members) with the same historical and RCP8.5 scenarios as for the CMIP5[45]. The sole difference across the members of the LE is a slight perturbation in the initial condition: each member is initialized with a random difference in atmospheric temperature ($\mathcal{O}10^{-14}$K). The second is a 10-member ensemble of atmosphere-only runs (Global Ocean Global Atmosphere, LE-GOGA), which are also forced by the historical and RCP8.5 scenarios between 1880-2015. In these simulations the sea surface temperature (SST) and sea-ice are prescribed based on the NOAA ERSSTv4[46] and the Hadley Centre HadISST[47] data sets, respectively. The third, is an ocean-atmosphere coupled 1800-year preindustrial control simulation (LE-PI); since the radiative forcing is fixed at year 1850, only internal variability is present in that simulation. The fourth experiment is an ocean-atmosphere coupled large ensemble that consists 20 members with the same historical and RCP8.5 scenarios as for the CMIP5 between 1920-2080, but without time-evolving greenhouse gases (LE-fixGHG).

Observations

Monthly mean near-surface air temperature (SAT) from all above reanalyses and CMIP5 models are validated against three different observed surface temperature data sets: the NOAAGlobal-Temp, the GISTEMP v3[48], and the HadCRUT4[49]. These data sets use a combination of satellite and in-situ measurements to produce global surface temperature over land and ocean.

Acknowledgements: RC is supported by the NOAA Climate and Global Change Postdoctoral Fellowship Program, administered by UCAR's Cooperative Programs for the Advancement of Earth System Science (CPAESS). LMP is founded by a grant from the National Science Foundation to Columbia University.

Data Availability: The data used in the manuscript is publicly available for CMIP5 data (https://esgf-node.llnl.gov/projects/cmip5/), CESM (http://www.cesm.ucar.edu/), ERA-I (https://www.ecmwf.int), NCEP2 (https://www.esrl.noaa.gov/psd/data/gridded/data.ncep.reanalysis2.html), JRA55, MERRA2 and CFSR2 (https://rda.ucar.edu/ and https://esgf.nccs.nasa.gov/projects/create-ip/).

Code Availability: Any codes used in the manuscript available upon request from rc3101@columbia.edu.

Author Contributions: R.C. downloaded and analyzed the data and together with L.M.P discussed and wrote the paper.

Competing Interests: The authors declare that they have no competing financial interests.

Correspondence: Correspondence and requests for materials should be addressed to rc3101@columbia.edu

References

1. IPCC. Summary of policymakers. *Climate Change 2013: The Physical Basis* (2013). T. F. Stocker et al., Eds., Cambridge University Press, 1-29.

2. Vallis, G. K., Zurita-Gotor, P., Cairns, C. & Kidston, J. Response of the large-scale structure of the atmosphere to global warming. *Q. J. R. Meteorol. Soc.* **141**, 1479–1501 (2015).

3. Francis, J. A. & Vavrus, S. J. Evidence linking Arctic amplification to extreme weather in mid-latitudes. *Geophys. Res. Lett.* **39**, L06801 (2012).

4. Liu, J., Curry, J. A., Wang, H., Song, M. & Horton, R. M. Impact of declining arctic sea ice on winter snowfall. *Proc. Natl. Acad. Sci. U.S.A.* **109**, 4074–4079 (2012).

5. Coumou, D., Petoukhov, V., Rahmstorf, S., Petri, S. & Schellnhuber, H. J. Quasi-resonant circulation regimes and hemispheric synchronization of extreme weather in boreal summer. *Proc. Natl. Acad. Sci. U.S.A.* **111**, 12331–12336 (2014).

6. Tang, Q., Zhang, X. & Francis, J. A. Extreme summer weather in northern mid-latitudes linked to a vanishing cryosphere. *Nature Cliamte Change* **4**, 45–50 (2014).

7. Barnes, E. A. Revisiting the evidence linking Arctic amplification to extreme weather in midlatitudes. *Geophys. Res. Lett.* **40**, 4734–4739 (2013).

8. Screen, J. A. & Simmonds, I. Exploring links between Arctic amplification and mid-latitude weather. *Geophys. Res. Lett.* **40**, 959–964 (2013).

9. Cohen, J. *et al.* Recent Arctic amplification and extreme mid-latitude weather. *Nature Geoscience* **7**, 627–637 (2014).

10. Screen, J. A., Deser, C., Simmonds, I. & Tomas, R. Atmospheric impacts of Arctic sea-ice loss, 1979-2009: separating forced change from atmospheric internal variability. *Clim. Dyn.* **43**, 333–344 (2014).

11. Vihma, T. Effects of Arctic Sea Ice Decline on Weather and Climate: A Review. *Surv. Geophys.* **35**, 1175–1214 (2014).

12. Walsh, J. E. Intensified warming of the Arctic: Causes and impacts on middle latitudes. *Glob. Planet. Chang.* **117**, 52–63 (2014).

13. Barnes, E. A. & Polvani, L. M. CMIP5 Projections of Arctic Amplification, of the North American/North Atlantic Circulation, and of Their Relationship. *J. Climate* **28**, 5254–5271 (2015).

14. Hassanzadeh, P. & Kuang, Z. Blocking variability: Arctic Amplification versus Arctic Oscillation. *Geophys. Res. Lett.* **42**, 8586–8595 (2015).

15. Blackport, R. & Kushner, P. J. The Transient and Equilibrium Climate Response to Rapid Summertime Sea Ice Loss in CCSM4. *J. Climate* **29**, 401–417 (2016).

16. Sun, L., Perlwitz, J. & Hoerling, M. What caused the recent "Warm Arctic, Cold Continents" trend pattern in winter temperatures? *Geophys. Res. Lett.* **43**, 5345–5352 (2016).

17. Simmons, A. J. & Hoskins, B. J. The life cycles of some nonlinear baroclinic waves. *J. Atmos. Sci.* **35**, 414–432 (1978).

18. Edmon, J. H. J., Hoskins, B. J. & McIntyre, M. E. Eliassen-palm cross sections for the troposphere. *J. Atmos. Sci.* **37**, 2600–2612 (1980).

19. Vallis, G. K. *Atmospheric and Oceanic Fluid Dynamics* (pp. 770. Cambridge University Press, Cambridge, U.K., 2006).

20. Yin, J. H. A consistent poleward shift of the storm tracks in simulations of 21st century climate. *Geophys. Res. Lett.* **32**, L18701 (2005).

21. Wu, Y., Ting, M., Seager, R., Huang, H. & Cane, M. A. Changes in storm tracks and energy transports in a warmer climate simulated by the GFDL CM2.1 model. *Clim. Dyn.* 203–222 (2010).

22. Oudar, T. *et al.* Respective roles of direct GHG radiative forcing and induced Arctic sea ice loss on the Northern Hemisphere atmospheric circulation. *Clim. Dyn.* **49**, 3693–3713 (2017).

23. Green, J. S. A. Transfer properties of the large-scale eddies and the general circulation of the atmosphere. *Q. J. R. Meteorol. Soc.* **96**, 157–185 (1970).

24. Held, I. M. The Vertical Scale of an Unstable Baroclinic Wave and Its Importance for Eddy Heat Flux Parameterizations. *J. Atmos. Sci.* **35**, 572–576 (1978).

25. Held, I. M. & Larichev, V. D. A scaling theory for horizontally homogeneous, baroclinically unstable flow on a beta plane. *J. Atmos. Sci.* **53**, 946–952 (1996).

26. Stone, P. H. Baroclinic adjustment. *J. Atmos. Sci.* **35**, 561–571 (1978).

27. Zurita-Gotor, P. The sensitivity of the isentropic slope in a primitive equation dry model. *J. Atmos. Sci.* **65**, 43–65 (2008).

28. Held, I. M. & O'Brien, E. Quasigeostrophic Turbulence in a Three-Layer Model: Effects of Vertical Structure in the Mean Shear. *J. Atmos. Sci.* **49**, 1861–1876 (1992).

29. Pavan, V. Sensitivity of a multi-layer quasi-geostrophic β-channel to the vertical structure of the equilibrium meridional temperature gradient. *Q. J. R. Meteorol. Soc.* **122**, 55–72 (1996).

30. Yuval, J. & Kaspi, Y. Eddy Activity Sensitivity to Changes in the Vertical Structure of Baroclinicity. *J. Atmos. Sci.* **73**, 1709–1726 (2016).

31. Jones, J. M. *et al.* Assessing recent trends in high-latitude Southern Hemisphere surface climate. *Nature Cliamte Change* **6**, 917–926 (2016).

32. Smith, K. L. & Polvani, L. M. Spatial patterns of recent Antarctic surface temperature trends and the importance of natural variability: lessons from multiple reconstructions and the CMIP5 models. *Clim. Dyn.* **48**, 2653–2670 (2017).

33. Kostov, Y., Ferreira, D., Armour, K. C. & Marshall, J. Contributions of Greenhouse Gas Forcing and the Southern Annular Mode to Historical Southern Ocean Surface Temperature Trends. *Geophys. Res. Lett.* **45**, 1086–1097 (2018).

34. Hawkins, E. & Sutton, R. Time of emergence of climate signals. *Geophys. Res. Lett.* **39**, L01702 (2012).

35. Deser, C., Terray, L. & Phillips, A. S. Forced and Internal Components of Winter Air Temperature Trends over North America during the past 50 Years: Mechanisms and Implications*. *J. Climate* **29**, 2237–2258 (2016).

36. Santer, B. D. *et al.* Identifying human influences on atmospheric temperature. *Proc. Natl. Acad. Sci. U.S.A.* **110**, 26–33 (2013).

37. Dee, D. P. *et al.* The ERA-Interim reanalysis: configuration and performance of the data assimilation system. *Q. J. R. Meteorol. Soc.* **137**, 553–597 (2011).

38. Kanamitsu, M. *et al.* Ncep-doe amip-ii reanalysis (r-2). *Bull. Am. Meteor. Soc.* **83**, 1631–1643 (2002).

39. Kobayashi, S. *et al.* The JRA-55 Reanalysis: General specifications and basic characteristics. *J. Meteor. Soc. Japan* **93**, 5–48 (2015).

40. Saha, S. *et al.* The NCEP Climate Forecast System Version 2. *J. Climate* **27**, 2185–2208 (2014).

41. Hines, K. M., Bromwich, D. H. & Marshall, G. J. Artificial Surface Pressure Trends in the NCEP-NCAR Reanalysis over the Southern Ocean and Antarctica. *J. Climate* **13**, 3940–3952 (2000).

42. Guo, Y. & Chang, E. K. M. Impacts of Assimilation of Satellite and Rawinsonde Observations on Southern Hemisphere Baroclinic Wave Activity in the NCEP NCAR Reanalysis. *J. Climate* **21**, 3290–3309 (2008).

43. Guo, Y., Chang, E. K. M. & Leroy, S. S. How strong are the Southern Hemisphere storm tracks? *Geophys. Res. Lett.* **36**, L22806 (2009).

44. Taylor, K. E., Stouffer, R. J. & Meehl, G. A. An Overview of CMIP5 and the Experiment Design. *Bull. Am. Meteor. Soc.* **93**, 485–498 (2012).

45. Kay, J. E. *et al.* The Community Earth System Model (CESM) Large Ensemble Project: A Community Resource for Studying Climate Change in the Presence of Internal Climate Variability. *Bull. Am. Meteor. Soc.* **96**, 1333–1349 (2015).

362 46. Huang, B. *et al.* Extended Reconstructed Sea Surface Temperature Version 4 (ERSST.v4).
363 Part I: Upgrades and Intercomparisons. *J. Climate* **28**, 911–930 (2015).

364 47. Rayner, N. A. *et al.* Global analyses of sea surface temperature, sea ice, and night marine air
365 temperature since the late nineteenth century. *J. Geophys. Res.* **108**, 4407 (2003).

366 48. Hansen, J., Ruedy, R., Sato, M. & Lo, K. Global Surface Temperature Change. *Rev. Geophys.*
367 **48**, RG4004 (2010).

368 49. Morice, C. P., Kennedy, J. J., Rayner, N. A. & Jones, P. D. Quantifying uncertainties in
369 global and regional temperature change using an ensemble of observational estimates: The
370 HadCRUT4 data set. *J. Geophys. Res.* **117**, D08101 (2012).

Figures

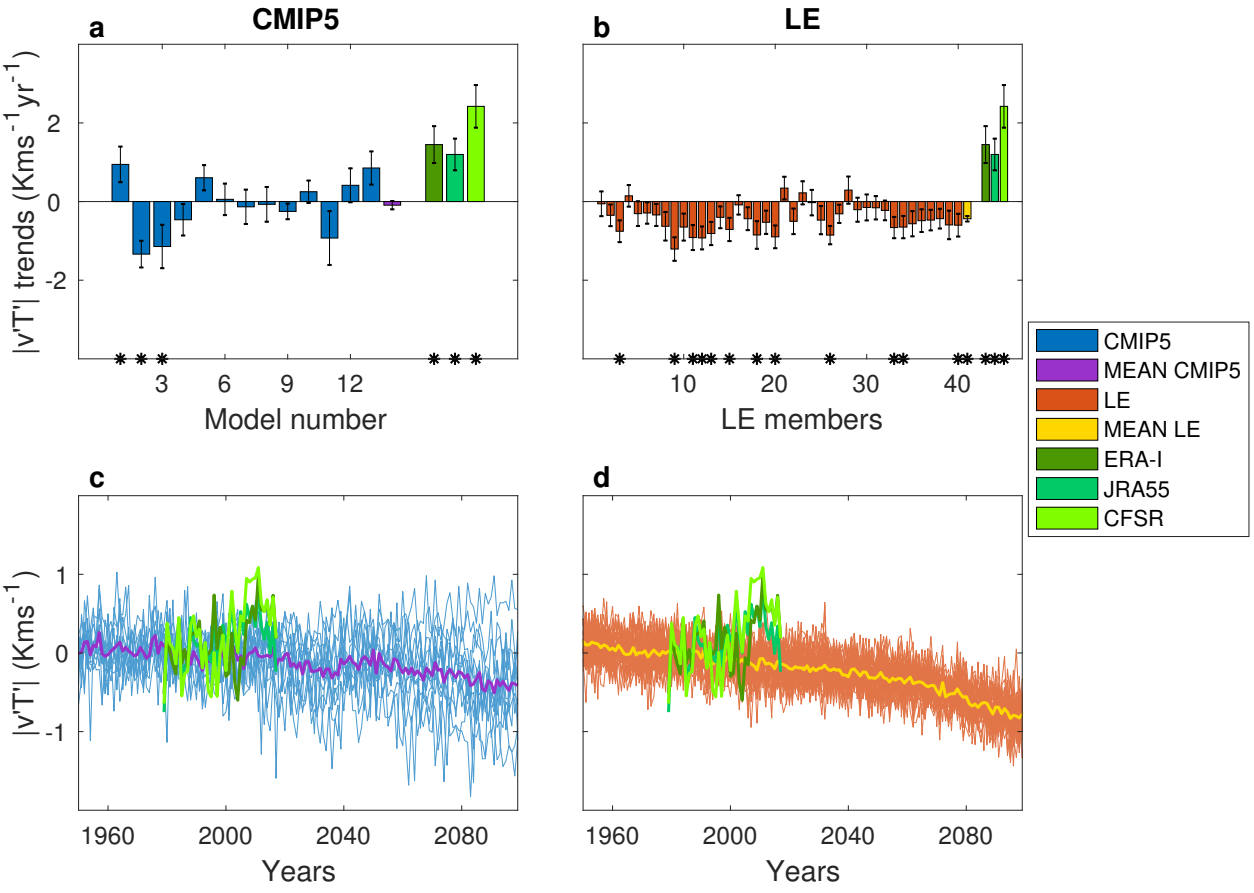

Figure 1: **SH $\overline{v'T'}$ trends and time series.** SH 39-year (1979-2017) trends (upper row, 10^{-2} $\mathrm{Kms^{-1}yr^{-1}}$) and time series, relative to the 1979-1989 period (bottom row, $\mathrm{Kms^{-1}}$), of $\overline{v'T'}$ in CMIP5 models (left column, blue colors with multi-model mean in purple) and LE members (right column, red colors with mean in yellow). In all panels green symbols represent the reanalyses. The asterisks in (a) and (b) indicate that the trends are statistically significant (p-values lower than 0.05), and the error bars show the standard error of linear regression coefficient.

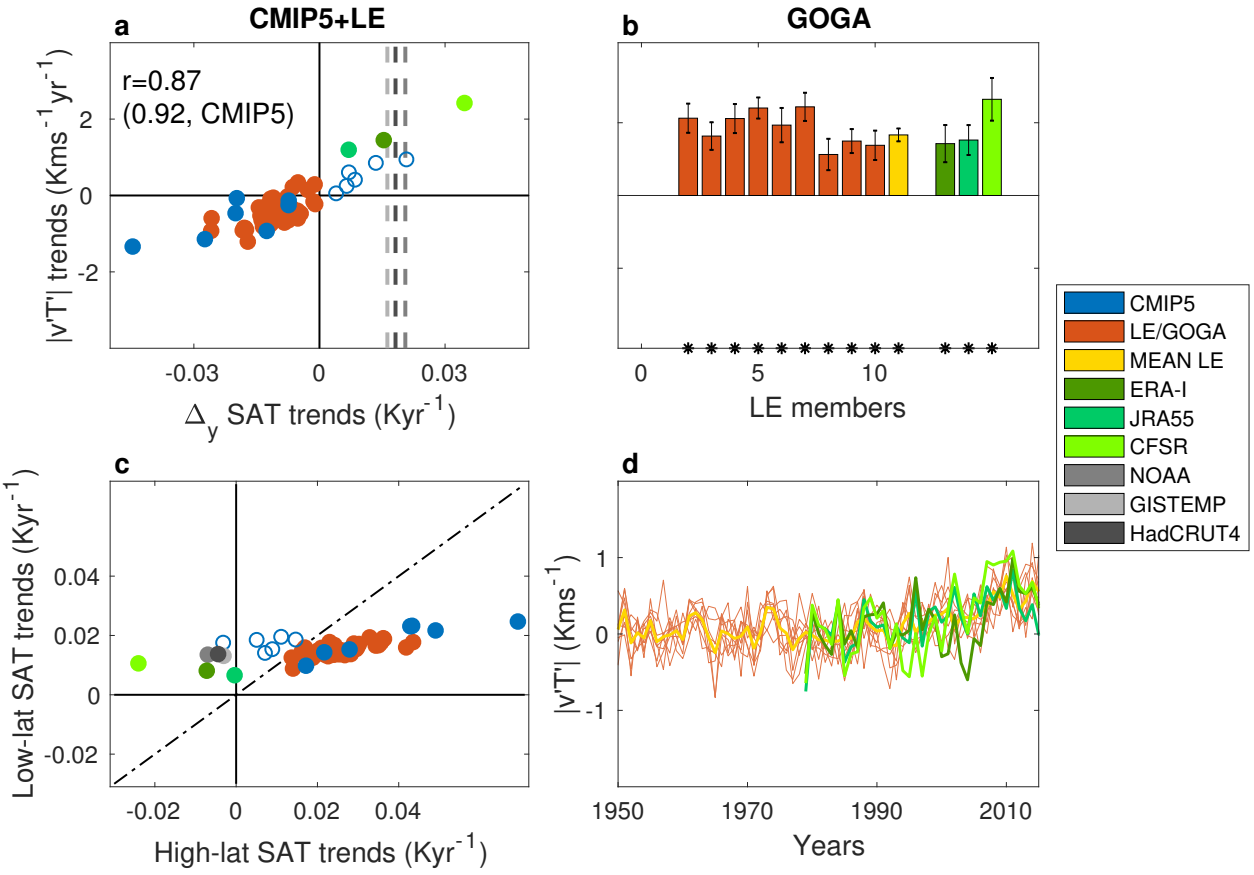

Figure 2: **SH $\overline{v'T'}$ and TAS relation.** (a) 39-year (1979-2017) trends in SH $\overline{v'T'}$ (10^{-2} $\mathrm{Kms^{-1}yr^{-1}}$) as a function of the trends in SH meridional gradient of SAT (Δ_ySAT). Correlations appear at the upper left corner. (b) 37-year (1979-2015) trends in SH $\overline{v'T'}$ (10^{-2} $\mathrm{Kms^{-1}yr^{-1}}$) in GOGA members. The asterisks in (b) indicate that the trends are statistically significant (p-values lower than 0.05), and the error bars show the standard error of linear regression coefficient. (c) 39-year (1979-2017) trends in SH low latitude SAT as a function of high latitude SAT trends. The dot-dashed line shows the 1:1 ratio. (d) Time series, relative to the 1979-1989 period, of SH $\overline{v'T'}$ in the GOGA simulations. In panels (a) and (c) blue, red, green and gray symbols represent the CMIP5 models, LE members, reanalyses, and observed SAT data sets, respectively. The open (filled) blue dots are CMIP5 models which simulate a strengthening (weakening) of SH $\overline{v'T'}$ over 1979-2017. In panels (b) and (d) red, yellow and green symbols represent the GOGA members, their mean, and the reanalyses, respectively.

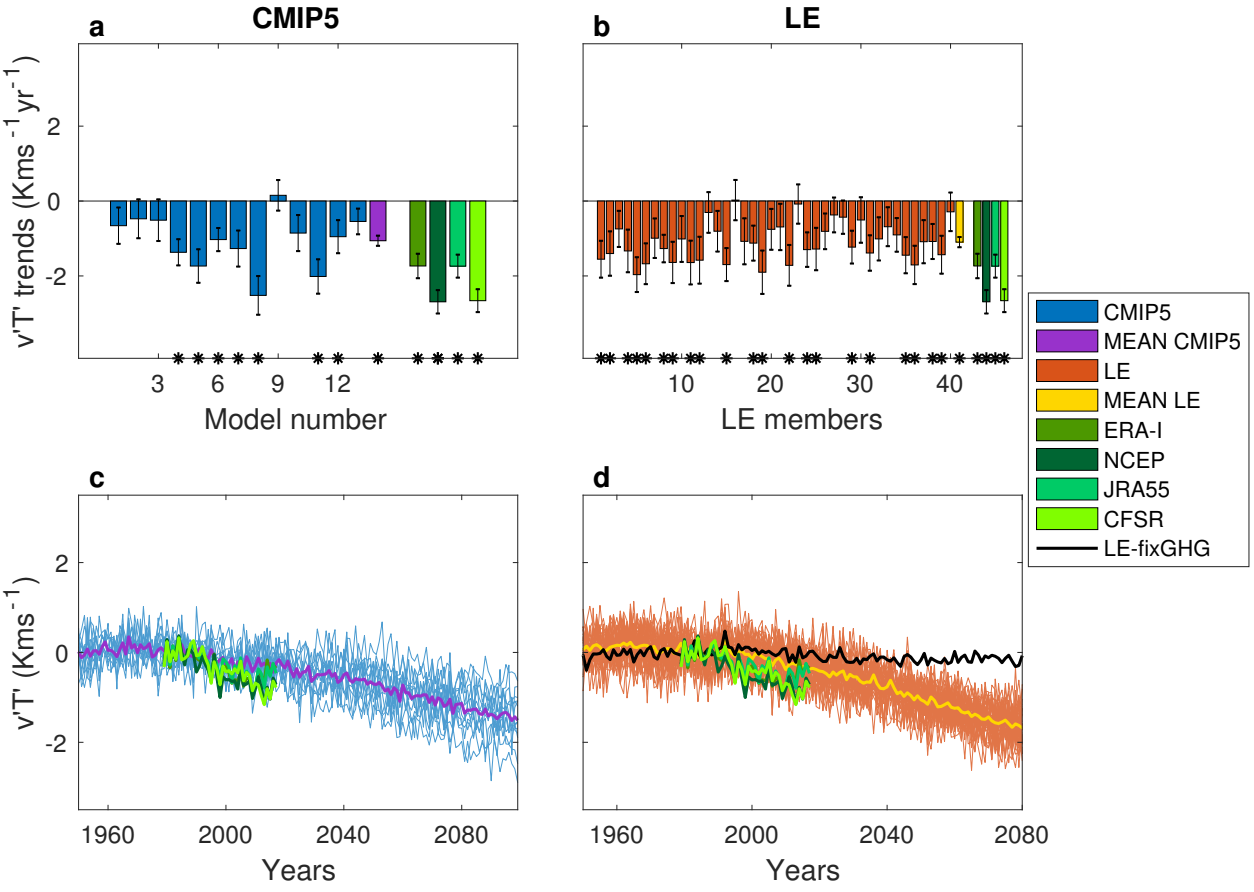

Figure 3: **NH $\overline{v'T'}$ trends and time series.** NH 39-year (1979-2017) trends (upper row, 10^{-2} $\mathrm{Kms^{-1}yr^{-1}}$) and time series, relative to the 1979-1989 period (bottom row, $\mathrm{Kms^{-1}}$), of $\overline{v'T'}$ in CMIP5 models (left column, blue colors with multi-model mean in purple) and LE members (right column, red colors with mean in yellow). In all panels green symbols represent the reanalyses. The asterisks in (a) and (b) indicate that the trends are statistically significant (p-values lower than 0.05), and the error bars show the standard error of linear regression coefficient. The black line in (d) shows the time series of mean LE-fixGHG simulation.

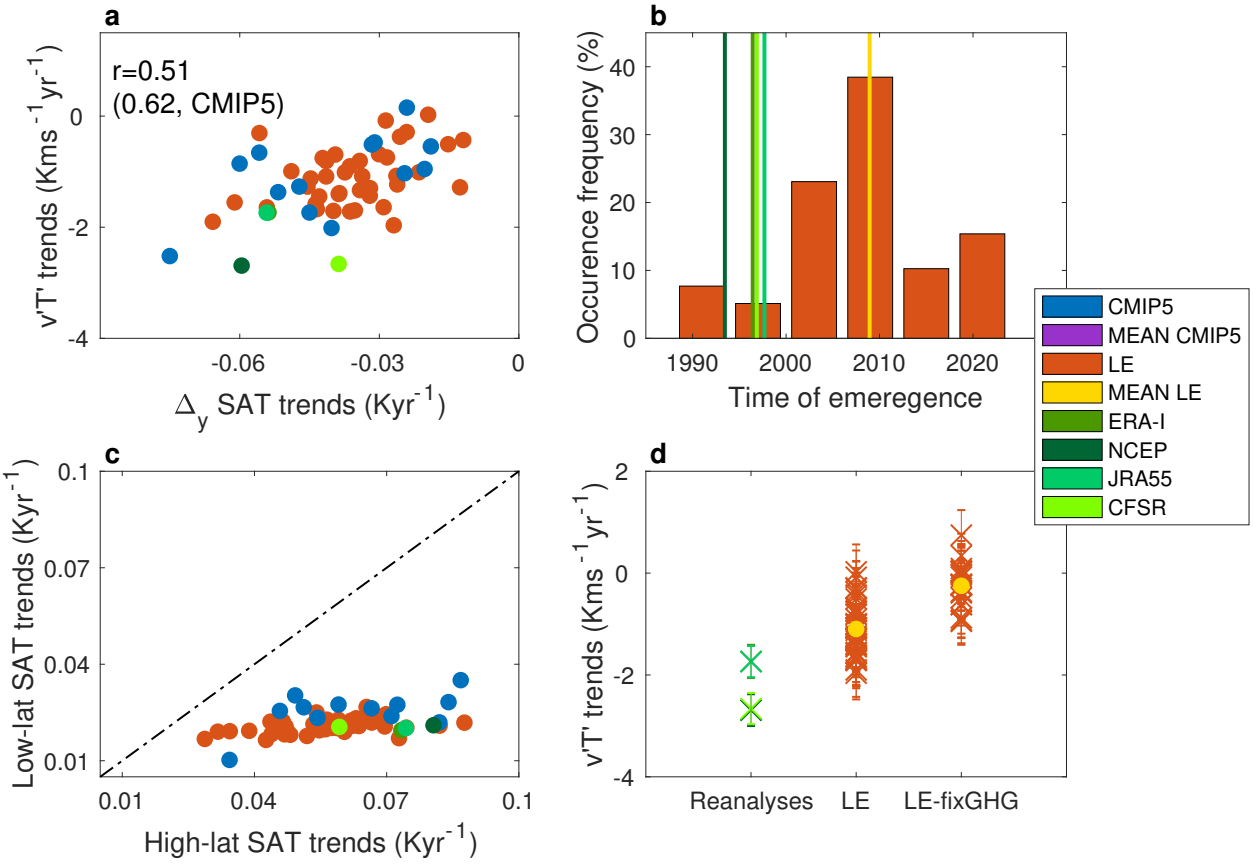

Figure 4: **Detection and attribution for NH $\overline{v'T'}$ and TAS relation.** (a) 39-year (1979-2017) trends in NH $\overline{v'T'}$ (10^{-2} $\mathrm{Kms^{-1}yr^{-1}}$) as a function of the trends in NH meridional gradient of SAT ($\Delta_y\mathrm{SAT}$). Correlations appear at the upper left corner. (b) The occurrence frequency (in percentage) of the time where the weakening of NH $\overline{v'T'}$ emerges out of the internal variability in the LE members (red bars). The vertical yellow and green lines show the time of emergence of the mean LE and reanalyses, respectively. (c) 39-year (1979-2017) trends in NH low latitude SAT as a function of high latitude SAT trends. The dot-dashed line shows the 1:1 ratio. (d) 39-year (1979-2017) trends in NH $\overline{v'T'}$ (10^{-2} $\mathrm{Kms^{-1}yr^{-1}}$) in reanalysis, LE and LE-fixGHG. The error bars show the standard error of linear regression coefficient. In panels (a) and (c) blue, red, and green symbols represent the CMIP5 models, LE members and reanalyses, respectively.